UDC 551.515.51:551.511.32:551.509.31

BAROTROPIC STABILITY AND TROPICAL DISTURBANCES

FRANK B. LIPPS

Geophysical Fluid Dynamics Laboratory, ESSA, Princeton University, Princeton, N.J.

ABSTRACT

This paper attempts to determine under what conditions horizontal shear in the mean zonal flow can provide the initial source of energy for the traveling disturbances of low latitudes. A three-zone barotropic model is constructed in order to examine the stability of an idealized mean zonal current. The width and total wind shear associated with this mean current are varied. The form of growing disturbances and their amplification rates are found.

A stability analysis is also carried out for a basic flow which has a hyperbolic tangent variation with latitude. Results obtained by numerical integration for this basic flow are similar to those found previously with the three-zone model. In discussing his easterly wave model, Yanai indicates a basic flow which has a total wind shear of about 8 m sec^{-1} occurring over approximately 6° of latitude. Results obtained for a basic flow with these characteristics show that the fastest growing wave has a wavelength near 2500 km and an e-folding time of about 7 days.

1. INTRODUCTION

One of the important unsolved problems in tropical meteorology is the formation of wavelike disturbances which can, under the right conditions, later develop into hurricanes. These disturbances propagate westward and often appear to have cold cores in the upper levels (Riehl 1954, Yanai 1961*a*). They are particularly noticeable along the intertropical convergence zones in the eastern Pacific and off the west coast of Africa where they seem to occur periodically with a spacing of about 1500–2000 km between disturbances. According to Sadler (1963), many of these disturbances in the eastern Pacific form along a wind-shear zone located near 10°–15° N.

If these disturbances have cold cores, it does not appear likely that they are maintained by a conversion of potential energy into kinetic energy. Yanai (1961*b*, 1964) has therefore suggested that they receive their energy from horizontal shear in the zonal flow and that the cold cores result from dynamically forced lifting associated with weak horizontal temperature gradients. That such a barotropic transfer of energy takes place is plausible when it is remembered that most of these disturbances occur along zones where strong horizontal shear exists. As suggested by Charney (1963), such shear can be expected across an ITCZ displaced from the Equator where air of differing absolute angular momentum converges.

However, there is also evidence that some disturbances are maintained by a baroclinic transformation of energy associated with the release of latent heat. Riehl (1967) discusses such a disturbance in the Caribbean. Underneath the altostratus or leaning cumulonimbus the air is cool and sinking, while in the clouds the air is warm and rising. The general circulation numerical calculations of Manabe and Smagorinsky (1967) also showed that tropical disturbances were maintained by the release of latent heat. Furthermore, Yanai (1968) states that the conversion of potential energy into kinetic energy in the upper troposphere cannot be ruled out for a synoptic case in the Caribbean. This case is similar in many respects to the case he previously discussed (Yanai 1961*a*), which apparently had a cold core in the upper levels.

Thus, the dynamics involved in the formation and maintenance of tropical disturbances is still an unsettled question. It is entirely possible that different disturbances are formed by different dynamical mechanisms. Of the different possible mechanisms, one can include 1) a barotropic transformation of energy associated with shear in the mean flow, 2) a baroclinic transformation of energy associated with release of latent heat, and 3) influences from middle latitudes. Undoubtedly, other possible mechanisms exist also. The purpose of the present investigation is to examine 1) above by means of a linear stability analysis. Although such an analysis greatly oversimplifies the actual atmospheric problem, it is hoped that the present results will give some indication as to when the barotropic transformation of kinetic energy from the basic flow to the disturbances can be dynamically important.

A barotropic stability analysis is carried out for two different forms of the mean flow. In the first case, the basic flow is split up into three latitude belts, the absolute vorticity being constant in each latitude zone. The width and total wind shear associated with this basic flow are varied. The form of growing disturbances and their amplification rates are obtained analytically.

The second type of basic flow studied has a hyperbolic tangent variation with latitude. The form of disturbances and their amplification rates are obtained by numerical integration. When both types of the basic flow have a similar latitudinal variation, the results of the stability analysis are similar. The hyperbolic tangent basic flow is used to simulate the mean flow given by Yanai (1961*b*) in discussing his easterly wave model. When this basic flow has a total wind shear of 8 m sec^{-1} occurring over approximately 6° of latitude, the most unstable disturbance has a wavelength near 2500 km and an e-folding time of about 7 days.

In a recent investigation, Nitta and Yanai (1968) obtained results from their barotropic stability analysis qualitatively similar to those obtained here for Yanai's

mean flow. The mean wind profiles used in their analysis were obtained from mean monthly data at or near the surface in the Marshall Islands. For the most unstable disturbances, they report e-folding times of 5.2 and 10 days for two different mean wind profiles. In both cases, the most unstable wavelength is in the range 2000–3000 km, and the disturbance has a southwest-northeast orientation.

In a very recent paper, Nitta and Yanai (1969) discuss in detail the results of their stability analysis for the June 1958 mean flow at the surface. For this case, the the most unstable wavelength is slightly longer than 2000 km, and the e-folding time is 5.2 days. The stream-function pattern is very similar to that found here. The primary difference between their results and the present results is that they have no long-wave cutoff for the unstable disturbances. It was found in the present analysis for Yanai's mean flow that the boundary at the Equator can make a significant change in the results. With walls at the Equator and 20° N. (as Nitta and Yanai have), it was found that the wave number of the marginally stable wave was reduced to half the value when no walls were present. Thus, the long waves may be unstable in Nitta and Yanai's analysis partly because of the wall at the Equator. Also, the fact that the mean flow has a somewhat different form may be a factor.

2. THE THREE-ZONE MODEL

In this section we construct a model consisting of three latitude belts in order to study the stability of infinitesimal disturbances superimposed on a basic current. This basic current is intended to simulate the mean flow associated with an ITC zone displayed to the north of the Equator. Such ITC zones are observed during the summer in the eastern Pacific and off the west coast of Africa. These are also the regions where many disturbances occur. The most important feature of the mean flow associated with such an ITC zone is the presence of a strong horizontal wind shear occurring over a few degrees of latitude. Since little is known about the exact form of these winds, an idealized model will be sufficient for present purposes. This model is similar to one examined by Queney (1952). Since his primary interest was in large-scale disturbances, his analysis was carried out on a sphere. The present analysis uses a beta plane.

The total flow is assumed to be horizontal, nondivergent, and barotropic. The present model, consisting of three zones (latitude belts), is shown in figure 1. Each zone has constant absolute vorticity so that the absolute vorticity is discontinuous between the different zones. The northern and southern zones are assumed to be infinite in extent. The central zone has a finite width a and is the one in which the strong shear in the mean flow takes place. The values of absolute vorticity for the southern, central, and northern zones are denoted respectively by $\bar{\zeta}_S$, $\bar{\zeta}_C$, and $\bar{\zeta}_N$. The value of the basic flow at the common

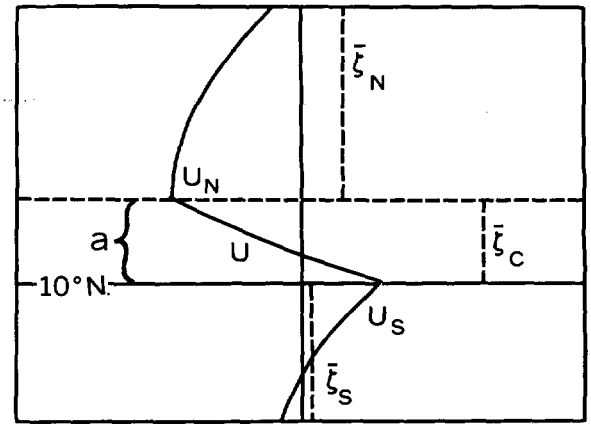

FIGURE 1.—Three-zone model. The discontinuous absolute vorticity is indicated by the dashed lines, and the mean current U is shown by the solid line. The width of the central zone is a.

boundary of the central and southern zones is U_S. Likewise, the value of the basic flow at the common boundary of the northern and central zones is U_N. The southern boundary of the central zone is held fixed at 10° N., and the value of U_N is given as -8 m sec^{-1}. The other parameters are varied in order to determine their importance to the stability problem.

In this way, a maximum amount of information can be obtained as to what parameters are important in determining the stability of disturbances. The two parameters held fixed cannot seriously change the characteristics of the stability problem. The specific value of U_N is unimportant since the stability of the basic flow is determined by its horizontal variation and not by its specific value at one point. Likewise, the exact latitude of the southern boundary of the central layer is unimportant, since β (the derivative of the Coriolis parameter f with latitude) is insensitive to small changes of latitude near 10° N. It is β and not f which is important to the present stability problem. Thus, we shall consider the variation of those parameters in the present model that are significant with respect to the stability of disturbances.

We now obtain the solution for the perturbation motion. A Cartesian coordinate system is used with the x-axis directed toward the east and the y-axis directed toward the north. The origin is assumed to be at 10° N. Since the flow is nondivergent, a stream function can be defined by

$$u=-\partial\psi/\partial y,\ v=\partial\psi/\partial x \tag{1}$$

where u and v are the disturbance velocities directed along the x-axis and y-axis, respectively. Since we are dealing with perturbed flow, we may assume that ψ is of the form

$$\psi=e^{ik(x-ct)}\phi(y) \tag{2}$$

where k is the wave number and c is the phase velocity, which is complex for unstable waves.

The stream function ψ must satisfy the vorticity equation in each of the three zones. In addition, the kinematic and dynamic boundary conditions must be satisfied on the two boundaries between the three zones. Since the absolute vorticity is a constant in each zone, the form of the vorticity equation in any zone is written

$$(U-c)(\partial/\partial x)\nabla^2\psi=0 \tag{3}$$

where U is the basic zonal current, ∇^2 is the Laplacian operator, and $\nabla^2\psi$ is the perturbation vorticity. The phase velocity c is complex for the solutions of interest (amplified waves) so that the perturbation vorticity must be zero in the interior of each zone. Thus, the following forms for solutions in the three zones may be obtained:

$$\phi_S(y)=Ae^{ky} \qquad -\infty<y\leq 0, \tag{4a}$$

$$\phi_C(y)=Be^{ky}+Ce^{-ky} \qquad 0\leq y\leq a, \tag{4b}$$

and

$$\phi_N(y)=De^{-ky} \qquad a\leq y\leq\infty \tag{4c}$$

where the subscripts S, C, and N represent respectively the southern, central, and northern zones where the solutions for ϕ are valid. Equations (4a) and (4c) already contain the requirement that the solutions damp out as $y\rightarrow\pm\infty$.

Since the basic velocity U is continuous between the different zones, the kinematic boundary condition at both internal boundaries is that the meridional velocity be continuous. The dynamic boundary condition is that the pressure be continuous across these boundaries. The perturbation pressure required for this boundary condition is obtained from the zonal equation of motion. For any of the three zones, the perturbation pressure p takes the form

$$(U-c)\frac{\partial\psi}{\partial y}+\psi\bar{\zeta}=p$$

where $\bar{\zeta}$ is the basic vorticity.

At $y=0$, the kinematic and dynamic boundary conditions give respectively

$$A=B+C \tag{5a}$$

and

$$k(U_S-c)(B-C-A)+A\Delta_0=0 \tag{5b}$$

where $\Delta_0=\bar{\zeta}_C-\bar{\zeta}_S$. Likewise at $y=a$ we find:

$$D=Be^{2ka}+C \tag{5c}$$

$$k(U_N-c)(-D-Be^{2ka}+C)+D\Delta_1=0 \tag{5d}$$

where $\Delta_1=\bar{\zeta}_N-\bar{\zeta}_C$. It should be noted here that $\bar{\zeta}_C$ is determined by the mean Coriolis parameter $\bar{f}$ in the central zone and the wind shear across this zone, that is,

$$\bar{\zeta}_C=\bar{f}-(U_N-U_S)/a. \tag{5e}$$

For a linearly varying f, the value of $\bar{f}$ is equal to the value of f at the midpoint of the zone.

We now have four homogeneous equations (5a–5d) for the four constants A, B, C, and D. In order for a nontrivial solution to exist, the determinant of the coefficients must vanish. This condition gives a quadratic equation for the phase velocity c. The solution for c is:

$$c=\frac{1}{2k}\left\{k(U_N+U_S)-\frac{1}{2}(\Delta_1+\Delta_0)\pm R^{1/2}\right\} \tag{6a}$$

and

$$R=\left[k(U_S-U_N)+\frac{1}{2}(\Delta_1-\Delta_0)\right]^2+\Delta_1\Delta_0e^{-2ka}. \tag{6b}$$

It is clear that c is complex only if R is negative. Thus the form of R shows that a necessary condition for unstable waves is that Δ_1 and Δ_0 be of opposite signs. In a fluid for which the absolute vorticity has a continuous variation, the necessary condition for instability is that the gradient of absolute vorticity change its sign somewhere in the fluid. Since $\Delta_0=\bar{\zeta}_C-\bar{\zeta}_S$ and $\Delta_1=\bar{\zeta}_N-\bar{\zeta}_C$, the condition that these be of opposite signs is a counterpart of the necessary condition for instability in a continuous flow field. Queney (1952) obtained the same necessary condition for instability as in the present study for his double-jet case.

In the present analysis for which $U_S>U_N$ and $\bar{\zeta}_C>\bar{\zeta}_S$, the necessary condition for unstable waves that Δ_1 and Δ_0 be of opposite signs is also a sufficient condition for instability. This follows from (6b), since with $U_S-U_N>0$ and $\Delta_0=\bar{\zeta}_C-\bar{\zeta}_S>0$ it can be seen that the term in brackets will vanish for some value of k when Δ_1 and Δ_0 are of opposite signs.

3. RESULTS OBTAINED FROM THE THREE-ZONE MODEL

In this section we discuss the solutions for the perturbed flow in the three-zone model. We first consider a basic flow that is assumed to be typical of conditions under which tropical disturbances may develop. Then we vary the parameters U_S, a, $\bar{\zeta}_S$, and $\bar{\zeta}_N$ to determine how the stability of disturbances is changed by changing the form of the basic flow. In this way it will be shown clearly which properties of the basic flow are important with respect to the stability of disturbances. The different forms of the basic flow studied are shown as eight cases in table 1. As mentioned previously, U_N is set equal to -8 m sec^{-1} for all eight cases. The first case will be used as a means of comparison for the remaining cases.

For this case we take the width a of the region of strong shear to be 3° of latitude. The total wind shear across this region is 13 m sec^{-1}, with U_S being 5 m sec^{-1} and U_N being -8 m sec^{-1}. The value of $\bar{\zeta}_S$ is taken as equal to the value of the Coriolis parameter f at 3° N. (0.7633×10^{-5} sec^{-1}), and the value of $\bar{\zeta}_N$ is taken as the value of f at 13° N. (0.3281×10^{-4} sec^{-1}). In this and most of the cases, $\bar{\zeta}_N$ was chosen so that dU/dy is zero at the southern boundary of the northern region. Figure 1 shows this type of zonal flow. The value of $\bar{\zeta}_C$ can be calculated from (5e). Assuming that f is linear in the central region, we find $\bar{\zeta}_C=0.6804\times10^{-4}$ sec^{-1}.

TABLE 1.—*Values of parameters used for each different basic flow*

Case no.	U_S (m sec^{-1})	a (° lat)	$\bar{\zeta}_S$ (sec^{-1})	$\bar{\zeta}_N$ (sec^{-1})
1	5	3	f at 3° N.	f at 13° N.
2	0	3	"	"
3	10	3	"	"
4	5	2	"	f at 12° N.
5	5	4	"	f at 14° N.
6	5	6	"	f at 16° N.
7	5	3	f at 6° N.	f at 13° N.
8	5	3	f at 3° N.	f at 17° N.

The results for case 1 are shown in table 2. The values of c_r and c_i were calculated from (6a) and (6b) for the 12 values of the wavelength λ shown in the first column of the table. The quantities AMP and T are defined by by AMP$=kc_i$ and $T=1/kc_i$. Physically, AMP is an amplification factor and T is the time it takes for a disturbance to amplify by a factor of e. The stable waves have two real phase velocities for each wavelength. For the unstable waves the two values of c are complex conjugates with one wave amplifying and the other damping. Only the amplifying modes are shown in table 2.

The data in this table show that the long and the short waves are stable. For the unstable waves, c_r is a linear function of the wavelength λ as can be inferred from the form of (6a). The most unstable disturbance has a wavelength of 2000 km and amplifies by a factor of $\bar{e}$ in 1.59 days. It travels westward with a phase speed of 3.50 m sec^{-1}.

The stream function for this unstable wave is shown in figure 2. The coordinates cover one wavelength in x and 10° of latitude in y. The basic flow is shown on the right. The streamlines are drawn at equal intervals on an arbitrary scale. The maximum amplitude of the disturbance occurs at 10° latitude, which is the boundary between the southern and central regions. The letters C and A represent the primary centers of cyclonic and anticyclonic vorticity. Secondary centers of vorticity are at the boundary of the central and northern regions. Note that for the three-zone model all of the disturbance vorticity occurs along the two boundaries of the central region.

This figure shows that the waves have a southwest-northeast orientation, which implies a northward transfer of momentum. That the disburbance gives such a transfer of momentum could be anticipated on general grounds. In this barotropic model, the total kinetic energy and the mean momentum of the zonal flow are conserved. The growing wave obtains its kinetic energy at the expense of the zonal kinetic energy. It is readily seen that for a zonal flow with a latitudinal variation, as in figure 2, there must be a northward transfer of momentum for the zonal flow to lose kinetic energy but conserve mean momentum.

We now consider the results for the remaining seven cases shown in table 1. For these cases, calculations were

TABLE 2.—*Results for case 1. In this table T is the e-folding time in days and* AMP *is the inverse of T.*

λ (km)	c_r (m sec^{-1})	c_i (m sec^{-1})	AMP (day^{-1})	T (day)
500	2.60	0	0	
	−6.60			
1000	0.16	0	0	
	−5.16			
1250	−1.24	0	0	
	−4.27			
1500	−3.00	1.11	0.401	2.50
1750	−3.25	1.93	.600	1.67
2000	−3.50	2.32	.630	1.59
2250	−3.75	2.52	.607	1.65
2500	−4.00	2.58	.561	1.78
2750	4.25	2.54	.502	1.99
3000	−4.51	2.41	.436	2.29
3500	−5.01	1.83	.283	3.53
4000	−4.83	0	0	
	−6.19			

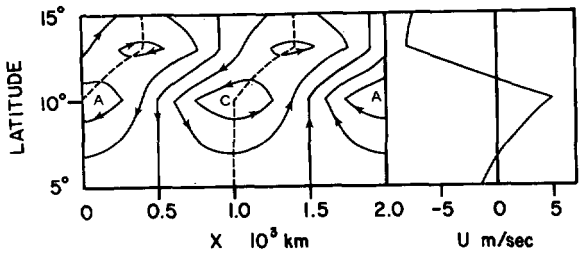

FIGURE 2.—Disturbance stream function for case 1 with $\lambda=2000$ km. The primary centers of cyclonic and anticyclonic vorticity are marked by C and A. The dashed line shows where the meridional velocity v vanishes. The basic flow is shown on the right.

carried out for the wavelengths shown in table 2. The most unstable wavelength, as well as c_r, c_i, AMP, and T for this wavelength, are shown in table 3 for all eight cases.

Cases 2 and 3 are the same as case 1 except that U_S is zero and 10 m sec^{-1}, respectively. A comparison of the amplification rates for the first three cases is shown in figure 3. Case 1 is shown as the solid line. It is seen that increasing U_S (and thus increasing the total shear across the central layer) increases the maximum amplification significantly. Also, the increase in shear leads to an increase in the wavelength of maximum amplification. Both of these changes seem to vary in a linear relationship with U_S.

We next determine the effect upon the growth rates of disturbances of varying the width of the central zone. In cases 4, 5, and 6, the width of the central region is 2°, 4°, and 6° of latitude, respectively. Otherwise, these cases are the same as case 1 with the value of the basic vorticity in the northern zone being set equal to the value of the Coriolis parameter at the southern boundary of this zone. The amplification rates as a function of wavelength are plotted in figure 4 for cases 1, 4, 5, and 6. It is readily

TABLE 3.—*Data for the most unstable wavelengths for all eight cases*

Case no.	λ (km)	c_r (m sec^{-1})	c_i (m sec^{-1})	AMP (day^{-1})	T (day)
1	2000	−3.50	2.32	0.630	1.59
2	1750	−5.75	1.14	.353	2.83
3	2250	−1.25	3.71	.896	1.12
4	1500	−2.85	2.72	.983	1.02
5	2500	−4.25	2.04	.443	2.26
6	3000	−5.39	1.34	.243	4.11
7	2250	−3.07	2.71	.654	1.53
8	2250	−4.63	2.50	.602	1.66

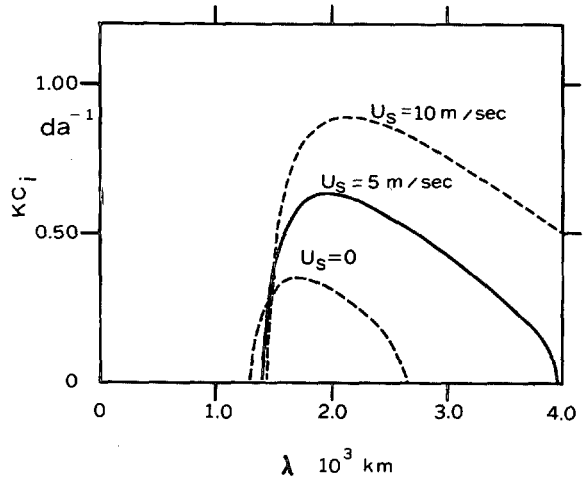

FIGURE 3.—Amplification rates as a function of U_S and λ. Shown are the amplification rates as a function of wavelength for case 1 (solid line) and cases 2 and 3 (dashed lines).

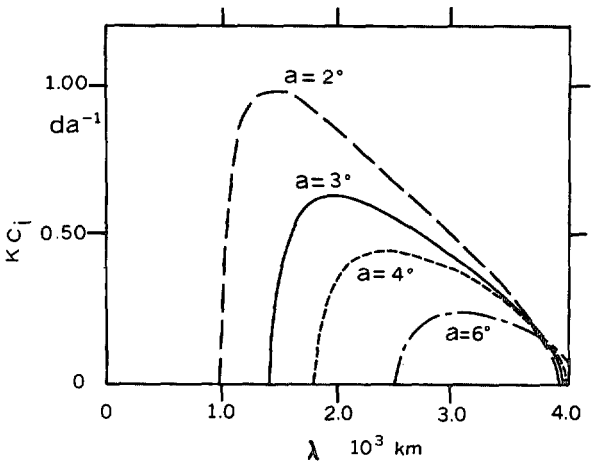

FIGURE 4.—Amplification rates as a function of a and λ. Shown are the amplification rates for case 1 (solid line) and cases 4, 5, and 6 (dashed lines).

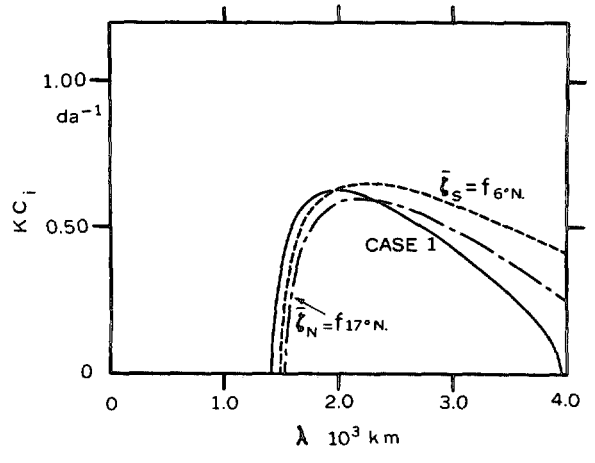

FIGURE 5.—Amplification as a function of $\bar{\zeta}_S$ and $\bar{\zeta}_N$. Shown are the amplification rates as a function of wavelength for case 1 solid line) and cases 7 and 8 (dashed lines).

seen that the maximum amplification increases and the wavelength of maximum growth rate decreases as the width of the central region is decreased.

The final two cases determine the effect of changing the value of absolute vorticity in the northern and southern zones but keeping the remaining parameters the same as in case 1. The seventh case has $\bar{\zeta}_S$ equal to the value of the Coriolis parameter f at 6° latitude. The final case has $\bar{\zeta}_N$ equal to the value of f at 17° latitude. (Case 1 has $\bar{\zeta}_S$ equal to the value of f at 3° latitude and $\bar{\zeta}_N$ equal to the value of f at 13° N.) The amplification rates for these two cases and for case 1 are plotted in figure 5. For some reason the form of the amplification curves for cases 7 and 8 are more similar to each other than they are to the curve for case 1. The maximum growth rate occurs at a wavelength of 2250 km for both of these cases, and the long waves are more unstable than for case 1. The maximum growth rates do not vary significantly from that for case 1.

In comparing figures 3, 4, and 5, it is seen that the most significant changes in the stability of disturbances are brought about by changing the total wind shear across the central zone and by changing the width of this zone. Changing the value of the absolute vorticity in the northern and southern zones has only a secondary effect upon the amplification rates of disturbances.

4. RESULTS FROM A CONTINUOUS MODEL

One objection that could be raised concerning the results of the last section is that the discontinuities of absolute vorticity in the three-zone model might give rise to unrealistic growth rates. In this section we give some results obtained by numerical integration for a basic flow which has a continuous vorticity distribution associated with it. The results obtained complement the previous results and indicate that the three-zone model gives sufficiently accurate results for the present purposes. The basic flow considered here will also be used to discuss the easterly wave model described by Yanai (1961*b*).

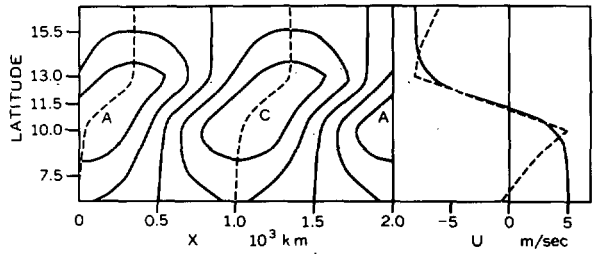

FIGURE 6.—Disturbance stream function for $B=0.06910$ with $\lambda=2000$ km. The centers of cyclonic and anticyclonic vorticity are marked by C and A. The dashed line shows where the meridional velocity v vanishes. On the right the solid line represents the basic flow for $B=0.06910$, and the dashed line represents the basic flow for case 1.

The form of the basic flow chosen is

$$U(y)=-U_0 \tanh (y/L)+U_1 \tag{7}$$

where U_0, U_1, and L are constants which need to be specified. Using the beta-plane approximation and equation (2) for the stream function, we find that $\phi(y)$ must satisfy

$$\frac{d^2\phi}{dy^2}-k^2\phi+\frac{\beta-d^2U/dy^2}{U-c}\phi=0 \tag{8}$$

where β is again the Rossby beta parameter. The boundary conditions are that $\phi\to 0$ as $y\to\pm\infty$.

The stability of this form of zonal wind profile has been studied by Michalke (1964) for the case $\beta=0$ and by Lipps (1965) with $\beta\neq 0$. Using numerical integration, Michalke found that the largest growth rate occurs for a nondimensional wave number α given by

$$\alpha=kL=0.4446. \tag{9}$$

If we assume that this wave number corresponds to a wavelength of 2000 km, we find that $L=141.5$ km. In order to have a basic flow that can be compared to case 1, we take the origin $y=0$ at 11.5° N. and set $L=141.5$ km, $U_0=6.5$ m sec^{-1}, and $U_1=-1.5$ m sec^{-1}. This basic flow is shown as the solid curve on the right in figure 6. The dashed curve is the basic flow associated with case 1. It is seen that the general shapes of these basic wind profiles are similar, with the largest difference occurring south of 10° N.

Numerical calculations were made to find the growth rates of disturbances with a finite β. The details of the calculations are given in the appendix. We mention here that equation (8) was nondimensionalized, split into real and imaginary parts, and put in finite-difference form. A total of 41 grid points was used with the centre of the grid at $y=0$. The grid-spacing was such that there were approximately 10 grid points in the interval $-1<y/L<+1$. On the northern and southern boundaries of this grid, the finite-difference solution was required to match with analytic solutions which damped out as $y\to\pm\infty$ outside the finite-difference mesh. A system of trial and error was used in order to find the correct complex phase velocity c that allowed the boundary conditions to be met. The wave number k was held fixed during this process.

Table 4.—*Comparison of the continuous model with the there-zone model for $\lambda=2000$ km*

	c_{r_r} (m sec^{-1})	c_i (m sec^{-1})	AMP (day^{-1})	T (day)
$B=0.06910$	−2.44	2.69	0.730	1.37
$B=0$	−1.50	2.77	.753	1.33
Case 1	−3.50	2.32	.630	1.59

The importance of β can be understood with the help of the nondimensional parameter B defined by

$$B=\beta L^2/U_0. \tag{10}$$

This is essentially the same parameter as the nondimensional beta defined in Lipps (1965). For the present problem, using the value of β at 11.5° N., $U_0=6.5$ m sec^{-1}, and $L=141.5$ km we find $B=0.06910$. Thus it seems that the effect of β should be small; however, it will be shown that even so small a value for B has a significant stabilizing effect on the long waves.

In table 4 it is seen that the effect of β is small for a wavelength of 2000 km. In this table we compare the results for $B=0.06910$ as obtained by the present numerical calculations with the results of Michalke ($B=0$) and with case 1. All these results are for a wavelength of 2000 km. These results show that the presence of β has a greater effect in causing the wave to progress westward due to a more negative c_r than in stabilizing the wave. Case 1 has the largest westward propagation. In comparison with case 1, the continuous model is somewhat more unstable. For $B=0.06910$ a disturbance with $\lambda=2000$ km will e-fold in 1.37 days, while for case 1 the value is 1.59 days.

In figure 6 we show the form of the disturbance stream function for $\beta=0.06910$ and $\lambda=2000$ km. The centers of cyclonic and anticyclonic activity are marked by C and A, respectively. The latitude range is from 6.06° to 16.94° N., the range of the numerical integration. When this figure is compared with figure 2, it is seen that the disturbance stream function has a similar pattern for both cases. In particular, it is noted that for both cases the disturbances tilt southwest-northeast in the region of strong shear, giving a northward transfer of momentum.

In addition to the case discussed above, numerical calculations were carried out for other wavelengths with $B=0.06910$. These are shown in table 5. In this table, α is the nondimensional wave number defined by $\alpha=kL$. In addition to the results obtained by numerical integration, the values of the marginally stable waves were obtained using the theory presented in Lipps (1965). The results in

TABLE 5.—*Values obtained for $B=0.06910$*

α	λ (km)	c_r (m sec^{-1})	c_i (m sec^{-1})	AMP (day^{-1})	T (day)
0.1875	4741	−7.88	0	0	
0.3	2964	−3.37	3.34	0.612	1.64
.4	2223	−2.64	2.93	.715	1.40
.4446	2000	−2.44	2.69	.730	1.37
.5	1778	−2.27	2.38	.728	1.37
.9994	890	−1.72	0		

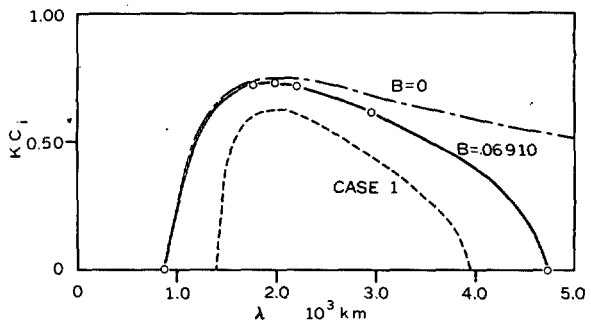

FIGURE 7.—Amplification as a function of wavelength for $B=0$, $B=0.06910$, and case 1. The solid line is $B=0.06910$ where the circles represent the data given in table 5. The values for $B=0$ are taken from Michalke (1964).

table 5 for the amplification rates are plotted in figure 7. In this figure, these values are compared with the values for $B=0$ (Michalke's data) and with case 1 of the three-zone model. The strong stabilizing effect of β on the long waves is very evident. For wavelengths of the order of 2000 km or less, the stabilizing effect of β is negligible. The amplification versus wavelength curve for case 1 has a shape very similar to that for $B=0.06910$ but with uniformly smaller amplification rates.

The above discussion and a comparison of figure 2 and figure 6 show that the results for case 1 of the three-zone model and for $B=0.06910$ with the present basic flow are similar. Thus, small changes in the form of the basic flow do not change the basic properties of the disturbances nor of the amplification as a function of wavelength. In particular, the discontinuities of absolute vorticity in the three-zone model do not appear to give rise to unrealistic results. Thus, we may conclude that the results of the three-zone model are sufficiently accurate for present purposes.

One of the interesting characteristics of the basic flow defined in equation (7) is that its latitudional variation appears similar in form to the basic flow discussed by Yanai (1961*b*). Figure 8 is taken from his paper and shows his idealized model of an easterly wave. The major difference between the horizontal variation of the basic flow shown in figure 8B and that shown in figure 6 is that the shear in Yanai's case apparently occurs over 5° to 6° of latitude instead of over 3° of latitude. Since this should approximately double the value of L, it is seen from equation (10) that B should increase by a factor of 4. Thus, the stabilizing effect of β should play a significant role for Yanai's case.

We now attempt roughly to simulate the form of basic flow discussed by Yanai. In the northern part of his figure, the basic flow $\bar{U}$ seems to approach −11 m sec^{-1}, and in the southern part it seems to approach −3 m sec^{-1}. Thus, it follows that we should set $U_0=4$ m sec^{-1} and $U_1=-7$ m sec^{-1}. The value for L is harder to determine and is more important as it occurs as L^2 in B. We take $L=261.4$ km. When we set β equal to its value at 10° N., we find $B=0.3849$. This value of B is half the value of B_{cr} for which the flow becomes stable (Lipps 1965). It is considered that this value for L gives a reasonable

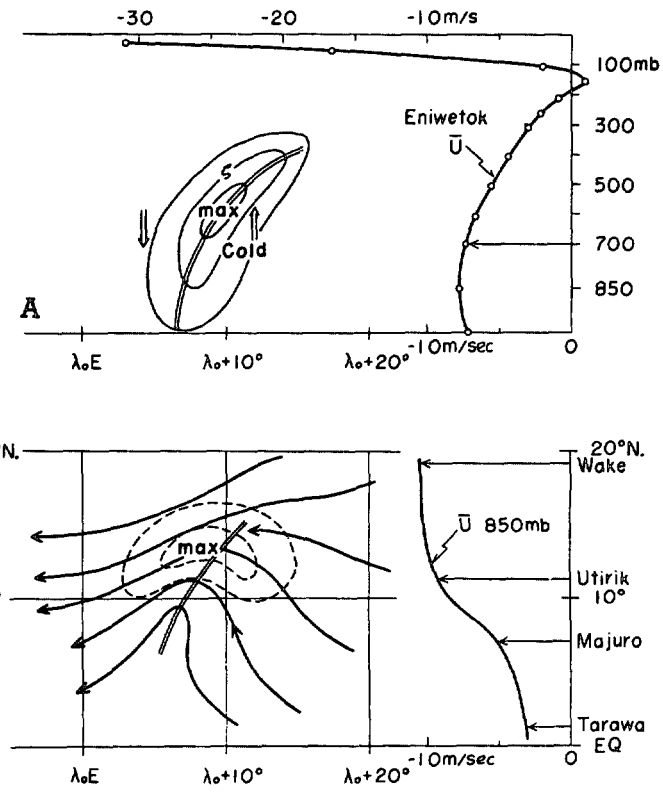

FIGURE 8.—Model of an easterly wave as presented by Yanai (1961*b*). (A) the schematic vertical structure of an easterly wave; thin lines are isolines of vorticity (left), and the vertical distribution of the mean zonal wind at Eniwetok Island in July 1958 is shown on the right. (B) the schematic horizontal view of an easterly wave; dashed lines are isovels (left), and the latitudinal distribution of the mean zonal wind at the 850-mb level is shown on the right.

shape to the basic flow profile. The origin $y=0$ is put at 10° N. This basic flow is shown on the right in figure 9.

In order to obtain information on the growth rates of disturbances, we again use numerical integration. The same procedure of integration is used here as was used for the previous case, except that now we set $B=0.3849$. Also, it turns out that for sufficient accuracy we may set

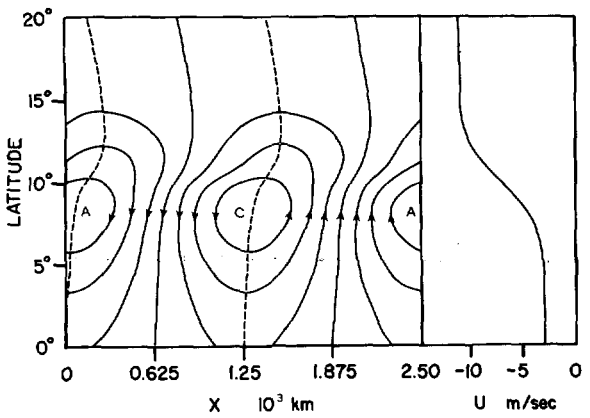

FIGURE 9.—The disturbance stream function for $B=0.3849$ and $\lambda=2500$ km ($\alpha^2=0.4325$). The notation is the same as for figures 2 and 6. The basic flow is shown on the right.

TABLE 6.—*Values obtained for $B=0.3849$*

α^2	λ (km)	c_r (m sec^{-1})	c_i (m sec^{-1})	AMP (day^{-1})	T (day)
0.9598	1676	−7.80	0	0	
.6670	2011	−8.15	0.35	0.095	10.50
.5000	2322	−8.45	.60	.140	7.14
.4325	2497	−8.65	.66	.144	6.96
.3610	2733	−8.96	.69	.136	7.34
.2175	3520	−10.54	0	0	

the disturbance stream function equal to zero at the northern boundary. This is discussed in the appendix. In the present set of integrations, the northern boundary is at 20° N., and the southern boundary is at the Equator.

The results are shown in table 6. The values for the marginal neutral waves are also given in this table. The numerical calculations were first carried out for $\alpha^2=0.667$, $\alpha^2=0.500$, and $\alpha^2=0.361$. From these results, it was estimated that the wave with the largest growth rate should be for $\alpha^2=0.4325$. Finally, calculations were done for this value of α^2. It is seen that the wavelength for this fastest growing wave is very nearly 2500 km and the e-folding time is very close to 7 days. The wave propagates westward with a phase speed of 8.65 m sec^{-1}.

The disturbance stream function for this wave is plotted in figure 9. It is seen that the wave tilts southwest-northeast in the region of strong basic flow shear. A small reverse tilt occurs farther north. This figure indicates qualitative agreement with Yanai's model of an easterly wave shown in figure 8B. It should be remembered that figure 8B shows the total flow, while the present figure shows only the disturbance flow. The strongest easterly winds should be to the north of the cyclonic center C in figure 9, where the disturbance easterlies combine with the basic flow easterlies to give a maximum in wind velocity. The southwest-northeast tilt of the wave near the center C also agrees with the tilt of the easterly wave indicated in figure 8B. The disturbances presented in figure 2 for case 1 and in figure 6 for $B=0.06910$ show a similar qualitative agreement with Yanai's model.

5. CONCLUDING REMARKS

In this investigation it is shown that the results are similar for case 1 of the three-zone model and for $B=0.06910$ with a hyperbolic tangent basic flow. The most unstable wavelengths are near $\lambda=2000$ km, and the e-folding time for these disturbances is about 1.5 days. For both of these cases the mean flow has a total wind shear of 13 m sec^{-1}, which occurs over a distance of about 3° latitude. If mean flows with these characteristics exist in the atmosphere, the present results suggest that the barotropic transformation of kinetic energy from the basic flow to the disturbances should be dynamically important. However, it should be noted that for the mean flows thus far observed in the Tropics the shear seems to be weaker than this value and to occur over larger latitude belts.

Results were obtained for $B=0.3849$, intended to simulate the mean flow given by Yanai (1961*b*). This basic flow has a total wind shear of 8 m sec^{-1}, which occurs over a distance of nearly 6° latitude. The most unstable wavelength is near $\lambda=2500$ km, and the e-folding time for this disturbance is close to 7 days. Similar results were obtained by Nitta and Yanai (1968) from their stability analysis of mean zonal currents in the Marshall Islands. The value of $\lambda=2500$ km may be too large. Furthermore, it is doubtful that an e-folding time of 7 days represents an amplification rate large enough to allow a small disturbance to overcome the effects of friction in the atmosphere and to increase in size.

Thus, the evidence is that the mean zonal winds obtained from mean monthly data in the Marshall Islands are only weakly unstable to barotropic disturbances. However, the zonal winds may vary significantly over a month, and the disturbances may develop when the winds are more unstable than indicated by their monthly average; but it is admitted that this is only a speculation. As indicated by the data of Alpert (1946), the eastern Pacific is another area that may become barotropically unstable in the summer. This is an area where many disturbances have been observed by TIROS satellites, as discussed by Sadler (1963, 1964) and Fujita et al. (1969) In the opinion of the present investigator, it is the eastern Pacific rather than the central Pacific where unstable barotropic disturbances are more likely to form along a shear zone.

APPENDIX

NUMERICAL PROCEDURE FOR THE CONTINUOUS BASIC FLOW

We discuss the numerical procedure used to obtain finite-difference solutions of equation (8) subject to the

TABLE 7.—*Data for $B=0.3849$ and $\alpha^2=0.4325$*

Case	c	kc_i
1	$-0.4133+0.1651i$	0.1086
2	$-.4135+.1654i$	.1088
3	$-.4143+.1657i$	.1090

boundary conditions that $\phi\to 0$ as $y\to\pm\infty$. The form of $U/(y)$ is given by equation (7). First we nondimensionalize the problem, using the characteristic velocity U_0 and the characteristic length L. We find

$$x^*=x/L,\ y^*=y/L,\ t^*=tU_0/L,\ \alpha=kL,$$

and

$$c^*=\frac{c-U_1}{U_0},\ B=\frac{\beta L^2}{U_0},\ U^*=-\tanh y^*,\ \phi^*=\frac{\phi}{U_0L} \tag{11}$$

where the asterisks represent nondimensional quantities. This nondimensionalization is very similar to that given by Lipps (1965). With the asterisks dropped, equation (8) becomes

$$\frac{d^2\phi}{dy^2}-\alpha^2\phi+\frac{B-d^2U/dy^2}{U-c}\phi=0 \tag{12}$$

where $U=-\tanh y$ as indicated by (11). The boundary conditions remain $\phi\to 0$ as $y\to\pm\infty$.

Equation (12) is solved numerically by using a 41-point grid mesh. The grid mesh is centered on the latitude for which $y=0$. Thus when grid points are labeled with the integer n, the grid point $n=21$ is placed at $y=0$. The grid interval is given by

$$\Delta y=0.21274$$

so that slightly less than 10 grid intervals cover the range $-1\le y\le+1$. The function $\tanh y$ has three-fourths of its total variation in this interval. The data shown in table 7 indicate that this resolution is sufficient, as only little change occurs with a doubled resolution.

Equation (12) is put in finite-difference form and separated into real and imaginary parts at interior grid points ($n=2$–40). The standard centered finite-difference form is applied to approximate $d^2\phi/dy^2$. The term $(B-d^2U/dy^2)/(U-c)$ is calculated exactly at each interior grid point.

At the boundaries the finite-difference solution is matched with analytic solutions that damp out as $y\to\pm\infty$. To a high degree of approximation, the basic flow outside the grid mesh is given by its limiting values. Thus, for the southern boundary, we match the finite-difference solution to the solution of

$$\frac{d^2\phi}{dy^2}-\alpha^2\phi+\frac{B}{1-c}\phi=0. \tag{13}$$

If we put

$$\phi=Ae^{py}, \tag{14}$$

we find

$$p=(\alpha^2-B/(1-c))^{1/2} \tag{15}$$

where the plus sign is chosen so that $\phi\to 0$ as $y\to-\infty$. To find the real and imaginary parts of p is straightforward but involves tedious algebra.

$$p=Re^{i\theta},\ c=c_r+ic_i,$$

$$F=\alpha^2-\frac{B(1-c_r)}{(1-c_r)^2+c_i^2},\ G=-\frac{Bc_i}{(1-c_r)^2+c_i^2},$$

and

$$R=(F^2+G^2)^{1/4},\quad \theta=0.5\tan^{-1}(G/F). \tag{16}$$

At the boundary grid point $n=1$, we are allowed to give ϕ_1 an arbitrary value. We find from equation (14) that

$$\phi_2/\phi_1=e^{p\cdot\Delta y} \tag{17}$$

so that given ϕ_1, the value ϕ_2 may be obtained. Next, ϕ_3, ϕ_4, . . . , ϕ_{41} are determined by the finite-difference form of (12). Finally, the computed value for ϕ_{41}/ϕ_{40} is compared with the required value of ϕ_{41}/ϕ_{40}. The required value of ϕ_{41}/ϕ_{40} is obtained from the analytic solution north of the finite-difference grid, which vanishes as $y\to+\infty$. This analytic solution is obtained in a manner similar to that discussed above.

While holding B and α fixed, the complex c is varied until the two values of ϕ_{41}/ϕ_{40} agree to sufficient accuracy. Several runs of the program must be computed in order to get successively better agreement. Once agreement is close enough, linear extrapolation may be applied using the analytic nature of ϕ_{41}/ϕ_{40} in the complex c plane. At this point convergence is rapid. Results gave values of c that were accurate to the fourth decimal place as far as the boundary conditions are concerned.

The above procedure was used for all values of B associated with $B=0.06910$. For $B=0.3849$ it was sufficient to set $\phi_{41}=0$, although it was still necessary to use the correct condition at the southern boundary for good accuracy. The solutions for which $\phi_{41}=0$ were obtained by a similar process of trial and error and linear extrapolation as discussed above.

In table 7, we show three cases to indicate the accuracy of the present numerical procedure. All three cases are for $B=0.3849$ and $\alpha^2=0.4325$, so that we are considering the fastest growing wave for Yanai's case. The wavelength is 2497 km. The data are in nondimensional form. The first case has 41 grid points and ϕ set to zero at the northern boundary. The second case has the correct northern boundary condition and 41 grid points. The final case has doubled the resolution (81 grid points) and has the correct northern boundary condition. It

is seen that the agreement is excellent. Another check on the numerical model was to calculate the wave numbers of the marginally stable waves for $B=0.3849$, which were previously obtained analytically by Lipps (1965). The numerical values and analytical values agree to the same accuracy as the data presented in table 7. A similar accuracy should be expected for the $B=0.06910$ calculations.

Finally, it is noted that the disturbance stream function shown in figure 9 was obtained from data given by case 2 with the correct northern boundary condition. The differences between the stream function data for cases 1 and 2 are negligible and show up only near the northern boundary.

ACKNOWLEDGMENTS

The author's initial interest in this problem was augmented by discussions with H. L. Kuo several years ago. Clem McGowan gave helpful programming assistance. Appreciation is expressed for those at the Geophysical Fluid Dynamics Laboratory who read the manuscript and made many helpful suggestions.

REFERENCES

Alpert, Leo, "The Inter-Tropical Convergence Zone of the Eastern Pacific Region, Part 2, "*Bulletin of the American Meteorological Society*, Vol. 27, No. 1, Jan. **1946**, pp. 15–29.

Charney, Jule C., "A Note on the Large-Scale Motions in the Tropics," *Journal of the Atmospheric Sciences*, Vol. 20, No. 6, Nov. **1963**, pp. 607–609.

Fujita, Tetsuya T., Watanabe, Kazuo, and Izawa, Tatsuo, "Formation and Structure of Equatorial Anticyclones Caused by Large-Scale Cross Equitorial Flows Determined by ATS–I Photographs," *SMRP Research Paper* No. 78, Satellite and Mesometeorology Research Project, Department of the Geophysical Sciences, University of Chicago, Jan. **1969**, 37 pp.

Lipps, Frank B., "The Stability of an Asymmetric Zonal Current in the Atmosphere," *Journal of Fluid Mechanics*, Vol. 21, Part 2, Feb. **1965**. pp. 225–239.

Manabe, Syukuro, and Smagorinsky, Joseph, "Simulated Climatology of a General Circulation Model With a Hydrologic Cycle: II. Analysis of the Tropical Atmosphere," *Monthly Weather Review*, Vol. 95, No. 4, Apr. **1967**, pp. 155–169.

Michalke, A., "On the Inviscid Instability of the Hyperbolic-Tangent Velocity Profile," *Journal of Fluid Mechanics*, Vol. 19, Part 4, Aug. **1964**, pp. 543–556.

Nitta, Tsuyoshi, and Yanai, Michio, "Barotropic Instability of the Equatorial Easterly Current," paper presented at the WMO/IUGG Symposium on Numerical Weather Prediction, Tokyo, Nov. 26–Dec. 4, **1968**.

Nitta, Tsuyoshi, and Yanai, Michio, "A Note on the Barotropic Instability of the Tropical Easterly Current," *Journal of the Meteorological Society of Japan*, Ser. 2, Vol. 47, No. 2, Apr. **1969**, pp. 127–130.

Queney, Paul, "Les ondes atmosphériques considérées comme associées aux discontinuités du torbillon," (Atmospheric Waves Associated With Velocity Discontinuities), *Tellus*, Vol. 4, No. 2, May **1952**, pp. 88–111.

Riehl, Herbert, "Waves in the Easterlies," *Tropical Meteorology*, McGraw-Hill Book Co., Inc., New York, **1954**, 392. pp., (see pp. 210–234).

Riehl, Herbert, "Varying Structure of Waves in the Easterlies," *Proceedings of the International Symposium on Dynamics of Large-Scale Atmospheric Processes, Moscow, USSR, June 23–30, 1965*, Izdatvo Nauka, Moscow, **1967**, pp. 411–416.

Sadler, James C., "Tiros Observations of the Summer Circulation and Weather Patterns of the Eastern North Pacific," *Report* No. 40, Contract No. AF19(604)–615b Hawaii Institute of Geophysics, Honolulu, **1963**, 47 pp.

Sadler, J. C., "Tropical Cyclones of the Eastern North Pacific as Revealed by TIROS Observations," *Journal of Applied Meteorology*, Vol. 3, No. 4, Aug. **1964**, pp. 347–366.

Yanai, Michio, "A Detailed Analysis of Typhoon Formation," *Journal of the Meteorological Society of Japan*, Ser. 2, Vol. 39, No. 4, Aug. **1961***a*, pp. 187–214.

Yanai, Michio, "Dynamical Aspects of Typhoon Formation," *Journal of the Meteorological Society of Japan*, Ser. 2, Vol. 39, No. 5, Oct. **1961***b*, pp. 282–309.

Yanai, Michio, "Formation of Tropical Cyclones," *Reviews of Geophysics*, Vol. 2, No. 2, May **1964**, pp. 367–414.

Yanai, Michio, "Evolution of a Tropical Disturbance in the Caribbean Sea Region," *Journal of the Meteorological Society of Japan*, Ser. 2, Vol. 46, No. 2, Apr. **1968**, pp. 86–109.

[*Received July 24, 1969; revised August 21, 1969*]